Climate Dynamics (2019) 52:3741–3757
https://doi.org/10.1007/s00382-018-4456-0

Reconstructing the western boundary variability of the Western Pacific Subtropical High over the past 200 years via Chinese cave oxygen isotope records

Jingyao Zhao[1] · Hai Cheng[1,2] · Yan Yang[3] · Liangcheng Tan[1,4] · Christoph Spötl[5] · Youfeng Ning[1] · Haiwei Zhang[1] · Xing Cheng[4] · Zhe Sun[3] · Xianglei Li[1] · Hanying Li[1] · Wen Liu[6] · R. Lawrence Edwards[2]

Received: 11 December 2017 / Accepted: 4 July 2018 / Published online: 21 September 2018

Abstract
Cave oxygen isotope ($\delta^{18}O$) records have been important in characterizing Asian Monsoon variations on a wide range of timescales. The climatic significance of the $\delta^{18}O$ proxy of the cave records and its main control factors, however, remain hotly debated, especially with respect to annual to decadal timescales. In particular, while the spatial and intensity variations of the Western Pacific Subtropical High (WPSH) affects the East Asian Monsoon remarkably on annual to decadal timescales, cave records up to present do not show clear evidence of the WPSH signal. Here we report a new high-resolution (average of 1.5 months) $\delta^{18}O$ record from Dongshiya Cave, Qinling Mountain, central China. The region is highly sensitive to variations in the position of the WPSH western boundary, which in turn regulates the alternation of dominant moisture sources between the proximal Pacific Ocean and the remote Indian Ocean. Together with another cave record near the WPSH western boundary, we established a new index to reconstruct variations of the WPSH western boundary over the past 200 years. Our new data revealed two significant periodicities, 12 and 2–7 years respectively, that can be causally linked to solar and ENSO variances correspondingly.

Keywords Speleothem · Oxygen isotopes · Asian Monsoon · WPSH

1 Introduction

Speleothem oxygen isotope ($\delta^{18}O$) records have been widely used to characterize Asian Monsoon (AM) variations on a wide range of timescales from orbital (e.g., Cheng et al. 2006, 2009a, 2016; Wang et al. 2008; Cai et al. 2015) and millennial (e.g., Wang et al. 2001; Cheng et al. 2009a; Yuan et al. 2004; Hu et al. 2008; Yang et al. 2010; Zhao et al. 2010; Jiang et al. 2016; Chen et al. 2016) to centennial-multidecadal (e.g., Fleitmann et al. 2003; Wang et al. 2005; Cheng et al. 2009b; Liu et al. 2013; Sinha et al. 2015; Tan et al. 2009, 2011, 2015) and decadal–annual (e.g., Zhang et al. 2008; Orland et al. 2015; Tan et al. 2014, 2016; Zhao et al. 2015; Li et al. 2017). While speleothem $\delta^{18}O$ variability has been widely attributed to changes in $\delta^{18}O$ of precipitation (e.g., Cheng et al. 2012, 2016; Tan 2009, 2011, 2013, 2016; Tan and Nan 2010; Tan et al. 2009, 2011, 2014, 2015, 2016; Duan et al. 2016), the climate interpretation of this isotope proxy remains a subject of intensive debate. The $\delta^{18}O$ variability on decadal to annual timescales has essentially been regarded as an expression of (a) the

✉ Hai Cheng
cheng021@xjtu.edu.cn

1 Institute of Global Environmental Change, Xi'an Jiaotong University, Xi'an 710054, China

2 Department of Earth Sciences, University of Minnesota, Minneapolis, MN 55455, USA

3 School of Geographical Sciences, Southwest University, Chongqing 400715, China

4 State Key Laboratory of Loess and Quaternary Geology, Institute of Earth Environment, Chinese Academy of Sciences, Xi'an 710061, China

5 Institute of Geology, University of Innsbruck, 6020 Innsbruck, Austria

6 Shandong Provincial Geo-mineral Engineer Exploration Institute, Jinan 250000, China

'amount effect' on the basis of an inverse correlation with the local–regional precipitation amount (e.g., Zhang et al. 2008; Zhao et al. 2015; Tan et al. 2009, 2011, 2014, 2015, 2016; Jiang et al. 2012; Goldsmith et al. 2017), or (b) the 'circulation effect', reflecting different moisture sources and trajectories controlled by different modes of atmospheric circulations (e.g., Tan 2009, 2011, 2013, 2016; Tan and Nan 2010; Dayem et al. 2010; Clemens et al. 2010; Pausata et al. 2011; Caley et al. 2014; Maher 2008).

The 'amount effect' interpretation of Chinese cave $\delta^{18}O$ records is somewhat perplexing. Indeed, statistically significant anti-correlations of speleothem $\delta^{18}O$ values and instrumental rainfall amount or wet/dry indexes were observed over the past ~ 60 years (e.g., Zhang et al. 2008; Zhao et al. 2015; Tan et al. 2009, 2016; Jiang et al. 2012; Li et al. 2017). However, this apparent 'amount effect' is essentially different from the sensu-stricto amount effect which refers to the observed decrease in rainfall $\delta^{18}O$ value with increased rainfall amount in tropics where deep convection events prevail (e.g., Dansgaard 1964; Rozanski et al. 1993). In the subtropical AM region, the apparent 'amount effect' observed for cave records is basically an overall negative correlation between the precipitation $\delta^{18}O$ and precipitation amount on annual to decadal timescales, which may be largely controlled by changes in moisture sources (e.g., Maher 2008; Maher and Thompson 2012; Dayem et al. 2010; Clemens et al. 2010), rather than the convectional amount effect mechanism. For instance, in the Asian summer monsoon fringe area (such as Wanxiang and Wuya caves), relatively more precipitation in summer time will increase the amount of precipitation with more negative $\delta^{18}O$ value originated from remote sources (Cheng et al. 2012), thus resulting in more negative weighted mean annual $\delta^{18}O$ as seen in Chinese cave records (e.g., Wang et al. 2001; Zhang et al. 2008; Tan et al. 2014; Cheng et al. 2009a, 2016).

More broadly on millennial–orbital timescales, Chinese cave records were commonly used as a proxy indicating the AM intensity in general (Cheng et al. 2012). Yuan et al. (2004) invoked the Rayleigh fractionation and suggested that changes in the fraction of water vapor rained-out along the moisture trajectory between tropical sources and the cave site could account to first order for the observed variability in the cave records. In addition, Cheng et al. (2009a, b) proposed that changes in the fraction of low $\delta^{18}O$ monsoon rainfall (or essentially summer rainfall) in annual totals could also explain the cave $\delta^{18}O$ records. Model studies actually support, rather than contradict, these ideas, although some of them emphasized the 'upstream depletion' instead of the 'local depletion' at cave site (e.g., Le Grande and Schmidt 2009; Pausata et al. 2011). In sum, for both model and observational results, the lower $\delta^{18}O$ implies higher spatially integrated monsoon rainfall between tropical monsoon sources and cave sites, and vice versa (Cheng et al. 2016).

Recently, Tan (2009, 2011, 2013, 2016) proposed a distinct 'circulation effect', which regards the Indian summer monsoon (ISM) as the main driver, bringing the remote moisture from the Indian Ocean to the monsoon region in eastern China. This occurred at times when the Western Pacific Subtropical High (WPSH) was weak and shifted eastward, and the moisture is thus characterized by the comparably low $\delta^{18}O$ values, reflecting large Rayleigh distillation along a longer trajectory. In contrast, when the WPSH strengthened and shifted westward, the East Asian summer monsoon (EASM) delivers more proximal moisture from the West Pacific Ocean and/or the South China Sea to eastern China, giving rise to higher precipitation $\delta^{18}O$ values. Indeed, the WPSH variability plays an important role in the climate regime of the Asian-Pacific region (e.g., Nitta 1987; Huang and Li 1989; Wu and Liu 2003; Wu et al. 2004; Wang et al. 2000, 2013; Liu et al. 2001; Xie et al. 2009; Zhou et al. 2009; Cao et al. 2009, 2012, 2016). In particular, the positive atmosphere–ocean feedback (Wang et al. 2000, 2013; Xie et al. 2009) and energy dispersion between the WPSH and the Indo-Pacific warm pool (Nitta 1987; Huang and Li 1989) are interactively connected with the AM system (Wu et al. 2004; Liu et al. 2001; Zhou et al. 2009; Cao et al. 2012, 2016; He and Zhou 2014, 2015a, b; He et al. 2015). As a result, a strong WPSH at more southwestern location may weaken the ISM over the Bay of Bengal, and strengthen the EASM over the South China Sea and the Western North Pacific, vice versa (e.g., Gong and Ho 2002; Zhou et al. 2009; Cao et al. 2012, 2016).

In order to gain further insights into the climate implication of cave $\delta^{18}O$ records in the EASM region, the high-resolution records with precise age control covering the recent decades are critical, because only these comparably young and high-resolution records can be directly and precisely compared to both instrumental data and meteorological observations, including the variability of the WPSH. Here, we present a high-resolution (~ 1.5 months) and well-dated $\delta^{18}O$ speleothem record from Dongshiya cave, Luanchuan, Henan Province, China, covering the last ~ 200 years. The cave is located in a key EASM area, close to the western boundary of the WPSH (Fig. 1). This unique setting allows us to test the 'circulation effect', because the precipitation $\delta^{18}O$ at this location is presumably much more sensitive to the WPSH position (Zhao et al. 2014) and, thus, to changes in the moisture sources and trajectories (the Indian Ocean vs. the Pacific Ocean/South China Sea). We explore the controlling factors of the $\delta^{18}O$ proxy on centennial to annual scales in the EASM region by comparing our new data and previous records from the region with instrumental data of the WPSH. On the basis of the comparison, we then reveal the WPSH variability over the last 200 years and the possible cause of it.

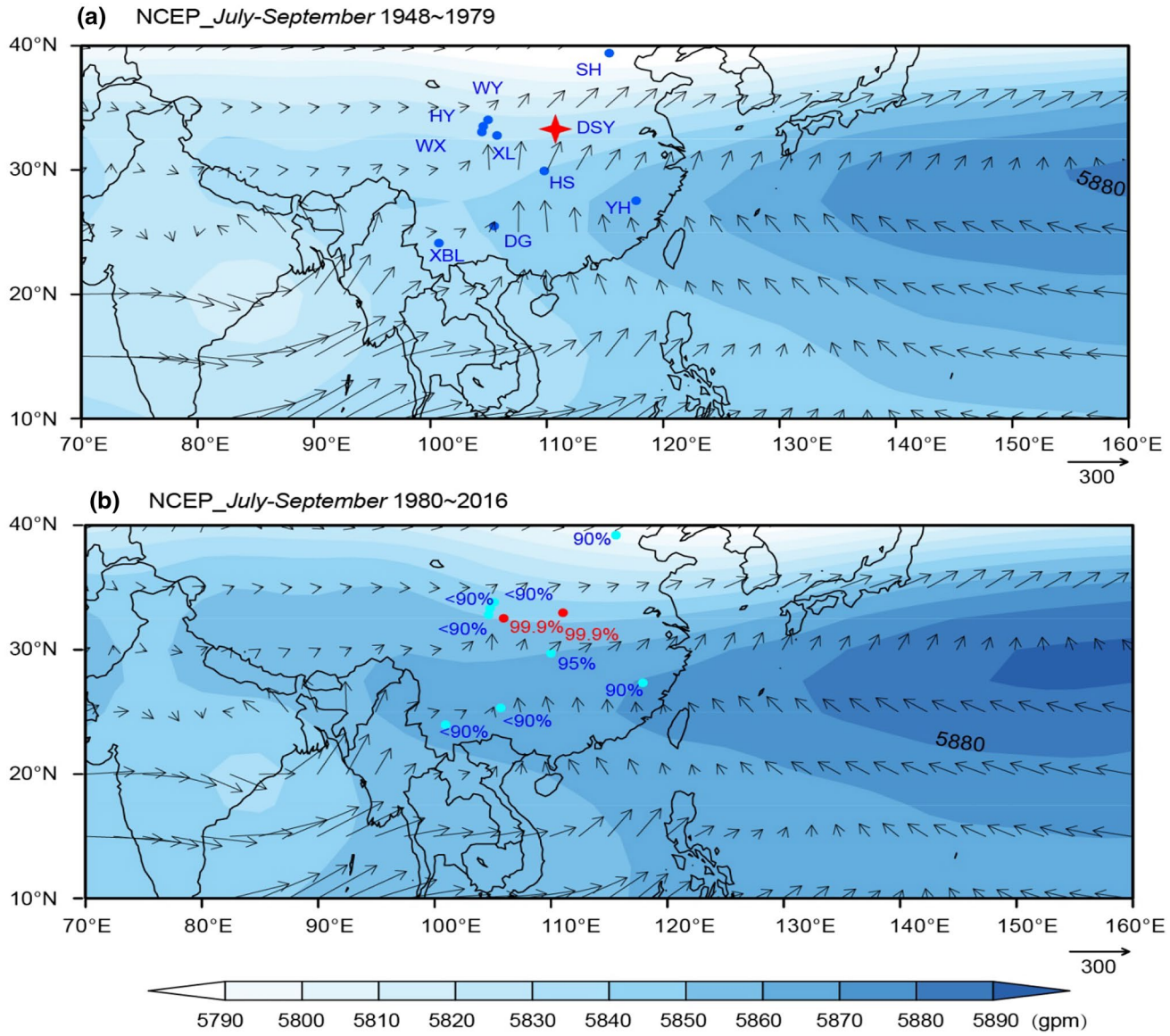

Fig. 1 Map of cave sites, moisture fluxes and geopotential heights. Cave sites (circles and labels), moisture fluxes integrated from 1000 to 300 hPa and geopotential heights at 500 hPa for July–September during 1948–1979 (**a**) and 1980–2016 (**b**), respectively. **a** Red star shows Dongshiya Cave. Blue circles depict cave locations: Shihua Cave (SH, Li et al. 2017), Xianglong Cave (XL, Tan et al. 2016), Dongge Cave (DG, Zhao et al. 2015), Wuya Cave (WY, Tan et al. 2014), Yuhua Cave (YH, Jiang et al. 2012), Huangye Cave (HY, Tan et al. 2011), Heshang Cave (HS, Hu et al. 2008), Wanxiang Cave (WX, Zhang et al. 2008), and Xiaobailong Cave (XBL, Tan et al. 2016). Numbers in **b** show the confidence levels of correlation coefficient between the cave $\delta^{18}O$ records and the changes of the WPSH western boundary (the WPSH data from NCCC: http://cmdp.ncc-cma.net/Monitoring/cn_index_130.php) (e.g., Zhao 1999; Zhou et al. 2009). Moisture fluxes (kg m^{-1} s^{-1}) and geopotential heights (gpm) are based on the monthly reanalyses data from the National Center for Environmental Prediction (NCEP) and the National Center for Atmospheric Research (NCAR)

2 Geological setting and sample collection

Dongshiya (DSY) Cave (111°34′E, 33°46′N, 840 m a.s.l.) and Jiguan Cave (900 m a.s.l.) (Fig. 1) are investigated in this study. The two caves (~300 m away from each other) are located in the Funiu Mountain in the eastern branch of the Qinling Mountains, ~5 km southwest of Luanchuan, central China. The host rock is the Cambrian limestone (Cai et al. 2008). The site is sensitively affected by both EASM and ISM with their relative strength linked closely to the position and intensity of the WPSH (Zhao et al. 2014). Most of the rainfall (~80%) in the area falls during the summer monsoon season (May–October). Mean annual temperature and precipitation recorded by a meteorological station ~5 km from the cave are 13.1 °C and 840 mm (1957–2014 AD), respectively. The vegetation above the cave is deciduous broad

leaf trees and shrubs. An active calcite stalagmite DSY1201, 14.0 cm in height and 7.5 cm in diameter, formed ~ 45 m behind the Dongshiya cave entrance. Another active calcite stalagmite, DSY1204, 60.9 cm in height and ~ 20.0 cm in diameter, was found ~ 110 m behind the entrance. Both samples were collected in April, 2012. Here we report the stable isotope record from stalagmite DSY1201, and use the DSY1204 record from the top 2.3 cm for a replication test. In addition, a monitoring work was carried out in Jiguan Cave from 2009 to 2017, which shows that the cave relative humidity was > 90%, and cave air temperature was 16.0 ± 2.0 °C (Sun 2017), close to the local mean annual air temperature at cave site.

3 Analytical methods

3.1 ^{230}Th dating

A total of 28 subsamples were drilled from a cut and polished slab of DSY1201 using the carbide dental burrs with diameters of 0.3–1.0 mm. The powdered subsamples were ^{230}Th-dated using multi-collector inductively coupled plasma mass spectrometry (Neptune Plus, Thermo-Scientific) in the Isotope Laboratory of Xi'an Jiaotong University, China. All errors are reported as 2σ. Standard chemistry procedures were used to separate U and Th (Edwards et al. 1987; Edwards 1988). A triple-spike (^{229}Th–^{233}U–^{236}U) isotope dilution method was employed to correct for instrumental fractionation and determine U/Th isotopic ratios and concentrations. The instrumentation, standardization, and half-lives are reported in Cheng et al. (2000, 2013). All U/Th isotopes were measured in peak-jumping mode on a MasCom multiplier placed behind the retarding potential quadrupole. We followed procedures to characterize the multiplier similar to those described in Cheng et al. (2000). Uncertainties in U/Th isotopic data were calculated offline, including corrections for blanks, multiplier dark noise, abundance sensitivity, and spike composition. ^{230}Th ages were corrected using an initial ^{230}Th/^{232}Th atomic ratio of $4.4 \pm 2.2 \times 10^{-6}$, a values for a material at secular equilibrium with the bulk earth ^{232}Th/^{238}U value of 3.8. The U and Th decay constants are reported in Cheng et al. (2013).

3.2 Layer counting

The Dongshiya stalagmites consist of couplets of a dark compact calcite (DCC) lamina, composed of micritic calcite, and a white porous calcite (WPC) lamina, composed of elongated columnar calcite (Fig. 2a) (cf. Genty and Quinif 1996; Frisia et al. 2000). The couplets, interpreted as annual cycles that formed in response to changing water excess (Genty and Quinif 1996; Mattey et al. 2008), were counted using high-resolution images obtained by a Zeiss AxioScope-A1 microscope in the Isotope Laboratory of Xi'an Jiaotong University. Couplets were counted six times by different people along the growth axis (Fig. 2a), giving the following results: 211, 204, 205, 201, 196 and 186 couplets, respectively. The average is 201 ± 16 (2σ). This number is consistent with the ^{230}Th dating results within uncertainties

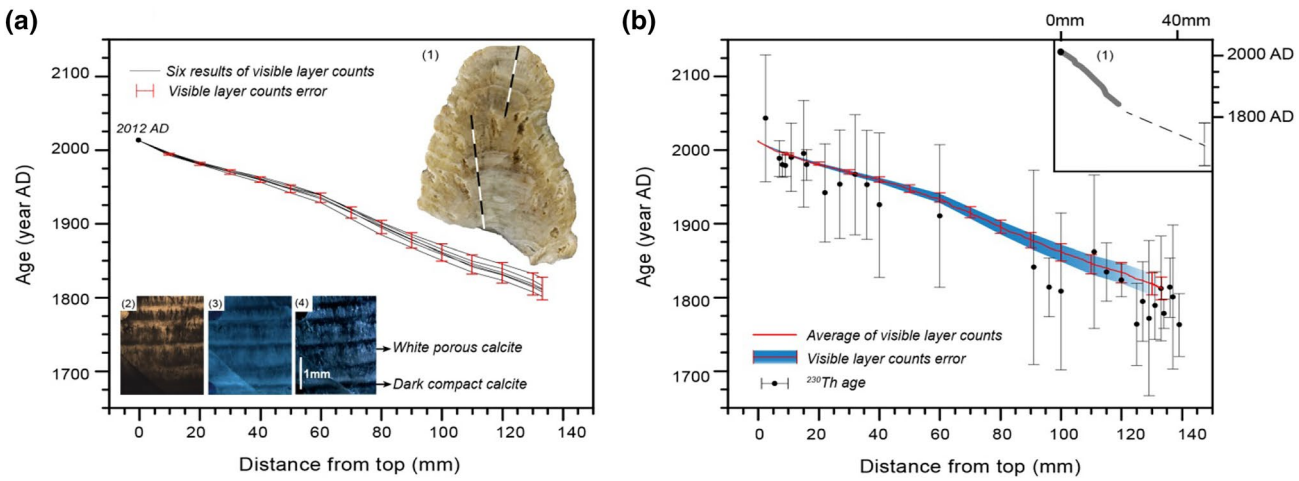

Fig. 2 Depth-age models of DSY1201. **a** Results of visible layer counting. The image 1 at the top right shows the polished slab of stalagmite DSY1201 with lamina counting and subsample (micromill) tracks (black and white lines). The images 2–4 at bottom left illustrate annual laminae composed of paired dark compact and white porous layers observed by transmitted light, epifluorescence and reflected light, respectively. **b** Age model based on ^{230}Th dates and visible annual layer counting statistics. Red line is the layer counting mean with the uncertainty indicated by the blue envelope. The insert plot shows the age model of stalagmite DSY1204 based on ^{230}Th dates and δ^{18}O correlations with the DSY1201record. The red and black error bars, respectively, show layer counting and ^{230}Th dating results errors (2σ)

(Fig. 2b), confirming that the couplet is annual. The counting results were applied to constrain the DSY1201 depth-age model accordingly (Fig. 2b).

3.3 Stable isotopes

Subsamples were micromilled perpendicularly to the extension axes of the stalagmites at 0.1 mm increment and analyzed using an on-line carbonate preparation system (Gasbench II) interfaced with an isotope ratio mass spectrometer (Delta^{plus} XL) at the University of Innsbruck. The long-term reproducibility is 0.06‰ and 0.08‰ (1σ) for $\delta^{13}C$ and $\delta^{18}O$ analyses, respectively (Spötl and Vennemann 2003). The spatial resolution at the top 10 mm was subsequently increased to 25 μm per sample, using a New Wave Research Micromill, and these samples were measured on a Thermo Scientific MAT 253 mass spectrometer coupled with an online carbonate preparation device (Kiel IV) at the Isotope Laboratory, Xi'an Jiaotong University. The typical analytical error (1σ) for $\delta^{18}O$ and $\delta^{13}C$ are 0.06‰ and 0.03‰, respectively (Li et al. 2017). A total of 1620 stable isotope data were obtained, and the international standards TTB1 and NBS18 were added to the analyses every 10–20 samples to check the reproducibility. Results from both laboratories are reported relative to the Vienna Pee Dee Belemnite (VPDB) standard.

Monitoring works in Jiguan Cave include stable isotopes analyses of modern calcite and cave drip water every 2 months over the past 8 years (2009–2017), as well as analyses of individual rainfall events. The results were reported in Zhao et al. (2014) and Sun (2017).

4 Results

4.1 Assessment of isotopic equilibrium during the calcite sample precipitation

Three methods were used to assess the isotopic equilibrium condition during speleothem formation. First, the broad resemblance of $\delta^{18}O$ records (Fig. 3) among the two stalagmites DSY1201 and DSY1204, as well as two previously published $\delta^{18}O$ records from Dongshiya and Laomu caves (Cai et al. 2008; Zhang et al. 2015) suggest that kinetic fractionation is negligible (Hendy 1971; Wang et al. 2001; Dorale and Liu 2009). Second, a comparison between $\delta^{18}O$ and $\delta^{13}C$ values along the growth axis of each speleothem shows no significant correlation ($r = 0.022$ for DSY1201) (Fig. 3). Finally, the results of another 'Hendy test' show that the $\delta^{18}O$ values remain virtually constant along eight growth layers of DSY1201 (Fig. 3). These lines of evidence suggest that the two stalagmites formed at or sufficiently

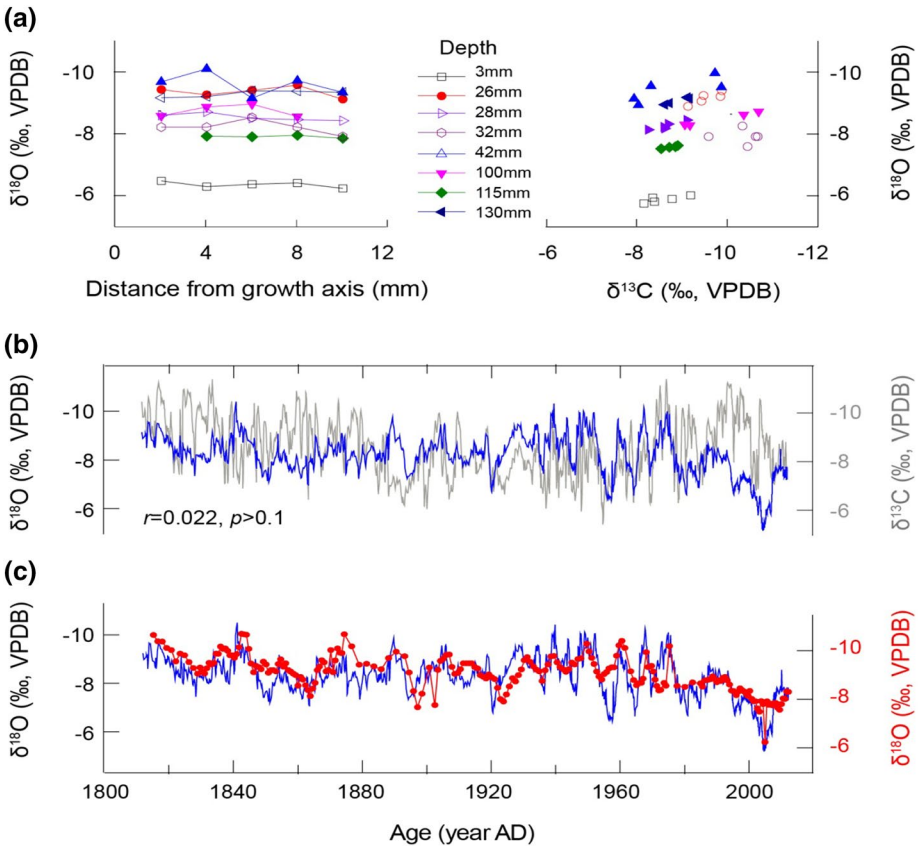

Fig. 3 Hendy test results. **a** $\delta^{18}O$ measurements along the same growth layer at eight different depths (left panel) and the plot of $\delta^{18}O$ vs. $\delta^{13}C$ for coeval subsamples (right panel). The $\delta^{18}O$ values in the same layer are virtually identical, and there are no significant correlations observed between $\delta^{18}O$ and $\delta^{13}C$ for coeval subsamples. **b** The comparison shows that the correlation between DSY1201 $\delta^{18}O$ and $\delta^{13}C$ is insignificant. **c** The comparison demonstrates a robust replication between DSY1201 (blue) and DSY1204 (red) $\delta^{18}O$ time series

close to isotopic equilibrium (Hendy 1971). Therefore, the isotope data primarily reflect the $\delta^{18}O$ value of meteoric precipitation.

4.2 DSY oxygen isotope time series

The new DSY $\delta^{18}O$ records cover the last ~ 200 years with an average resolution of ~ 1.5 months (Fig. 3). The $\delta^{18}O$ values range from − 5.3 to − 10.6‰ (average − 8.8‰), and $\delta^{13}C$ varies from − 5.6 to − 11.6‰ (average − 9.7‰). The DSY record is characterized by a persistent decadal oscillation over the last 200 years (Fig. 3). The $\delta^{18}O$ record also reveals a progressively increasing trend, particularly after the late 1970s (Fig. 3). This trend has been previously documented for the East Asian climate, particularly for the WPSH intensity, size and location since the late 1970s (e.g., Gong and Ho 2002; Zhou et al. 2009; He et al. 2015; Huang et al. 2016).

The very high growth rates (~ 0.67 ± 0.05 mm year^{-1}) of the DSY stalagmite samples allow us to obtain an unprecedently high temporal resolution (seasonal to monthly) record. The large amplitude of the $\delta^{18}O$ record is consistent with the range of the modern calcite $\delta^{18}O$ values (− 5.0 to − 10.1‰) as observed from our monitoring work between 2009 and 2017.

5 Discussion

5.1 Comparison between variances of the WPSH and Chinese cave $\delta^{18}O$ records

As summarized in a recent study by Li et al. (2017), several high-resolution (better than 2-years) cave $\delta^{18}O$ records from different locations of the EASM region demonstrate an increasing trend since the late 1970s, including Yuhua (Jiang et al. 2012), Heshang (Hu et al. 2008), Wuya (Tan et al. 2014), Xianglong (Tan et al. 2015) and Shihua (Li et al. 2017) cave records from both North and South China (Figs. 1, 4). Principal Component Analysis (PCA) of these cave records reinforces the observation (Fig. 4). Nevertheless, the spatial pattern of summer rainfall between North and South China is generally different as demonstrated by both instrumental records and precipitation reconstructions in the EASM region of eastern China (e.g., Tao and Chen 1987; Gong and Ho 2002; Ding et al. 2008; He et al. 2017). Thus, there exists a paradox of a consistent trend in cave records, but different summer rainfall amounts in other observational/instrumental data between North and South China.

Previous studies have shown that the WPSH intensification and/or its westward extension since the late 1970s have profoundly contributed to the decadal variability of the

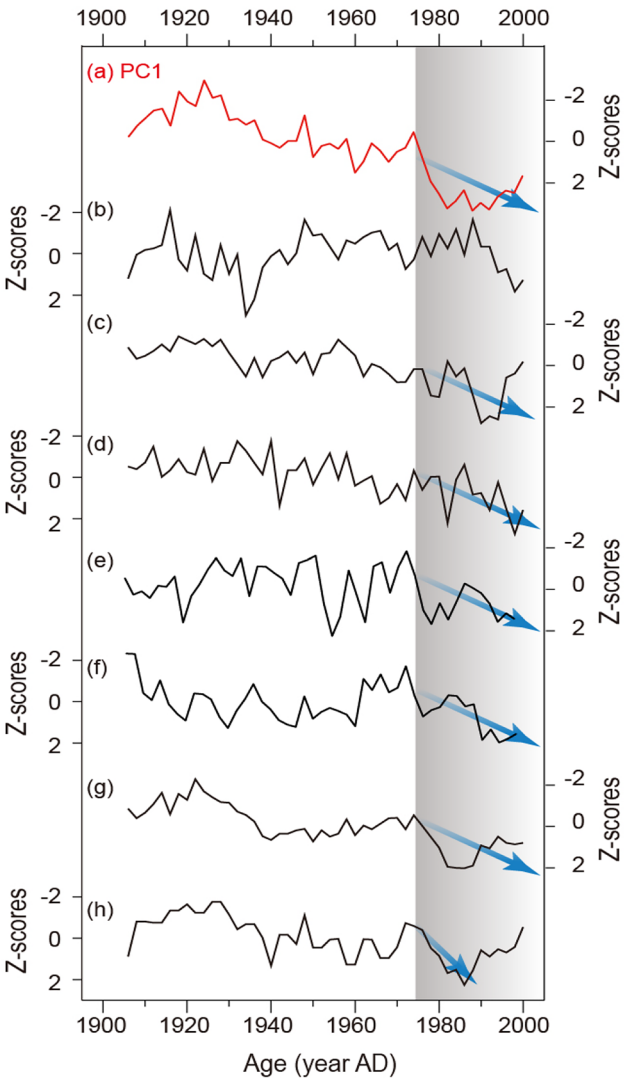

Fig. 4 High-resolution speleothem $\delta^{18}O$ records from China over the last century. All the selected records have resolutions higher than 2 years. Red line (**a**) represents the Principal Component 1 of the speleothem records. All time series are normalized to the standard Z-scores, using the software Origin Pro 2016 (http://www.originlab.com/), in order to show variations. Black curves represent $\delta^{18}O$ records from Wanxiang Cave (**b**) (Zhang et al. 2008), Shihua Cave (**c**) (Li et al. 2017), Wuya Cave (**d**) (Tan et al. 2014), Dongshiya Cave (**e**) (this study), Xianglong Cave (**f**) (Tan et al. 2016), Heshang Cave (**g**) (Hu et al. 2008) and Yuhua Cave (**h**) (Jiang et al. 2012). Blue arrows show the progressive westward shift of the WPSH since the late 1970s

East Asian climate (e.g., Hu 1997; Wang et al. 2000, 2013; Gong and Ho 2002; Zhou et al. 2009). Although the spatial extent of the WPSH varies depending on its definition (e.g., Huang et al. 2016; He and Zhou 2015b; Yang et al. 2017), it is generally accepted to use the contour line of 5880 geopotential meters (gpm) to define the spatial boundary of the WPSH (Fig. 1), which is also routinely used by the National Climate Center of China (NCCC). As such, the westernmost

longitude of the western boundary of 5880 gpm was applied in this study to define the western extent of the WPSH. On the basis of this definition, the dramatic WPSH enhancement since the late 1970s is mirrored by the increasing trend in the cave $\delta^{18}O$ records (Fig. 4). Statistical analyses also show that the WPSH variations during the last ~ 60 years are significantly correlated with a set of cave $\delta^{18}O$ records, such as Heshang ($r = 0.32$, $p < 0.05$), Xianglong ($r = 0.59$, $p < 0.001$) (Fig. 5) and Dongshiya ($r = 0.46$, $p < 0.001$). This is consistent with the aforementioned 'circulation effect' (Tan 2009, 2011, 2013, 2016), because WPSH variations are strongly coupled with atmosphere circulation changes. However, WPSH variations do not correlate significantly to a set of other cave $\delta^{18}O$ records, such as Wanxiang ($p > 0.1$), Wuya ($p > 0.1$), Huangye ($p > 0.1$), Xiaobailong ($p > 0.1$) and Dongge ($p > 0.1$), or show a rather weak correlation (at low confidence levels) with the Yuhua ($p < 0.1$) and Shihua ($p < 0.1$) records (Fig. 5).

A close look at the geographic locations of the caves reveals that those cave records that highly correlate with changes in the WPSH are from central China (Figs. 1, 5). The 'circulation effect' therefore can well explain the cave $\delta^{18}O$ records from the region where the alteration is considerable between the two major summer monsoon moisture sources (the Indian Ocean vs. the Pacific/South China Sea). For example, the DSY Cave in the Qinlin region which is geographically located between North and South China with an annual precipitation of ~ 800 mm year^{-1}, close to the average in the EASM region of eastern China. In fact, it was previously demonstrated that the precipitation $\delta^{18}O$ in the area appears to be more sensitive to changes in moisture sources than precipitation amount (Zhao et al. 2014). This is probably because annual precipitation amount in central eastern China varies smaller than those in North and South China, in accordance with the precipitation anomalies in eastern China that tend to be have a pattern of 'southern flood and northern drought' (and vice versa) or a 'dipole

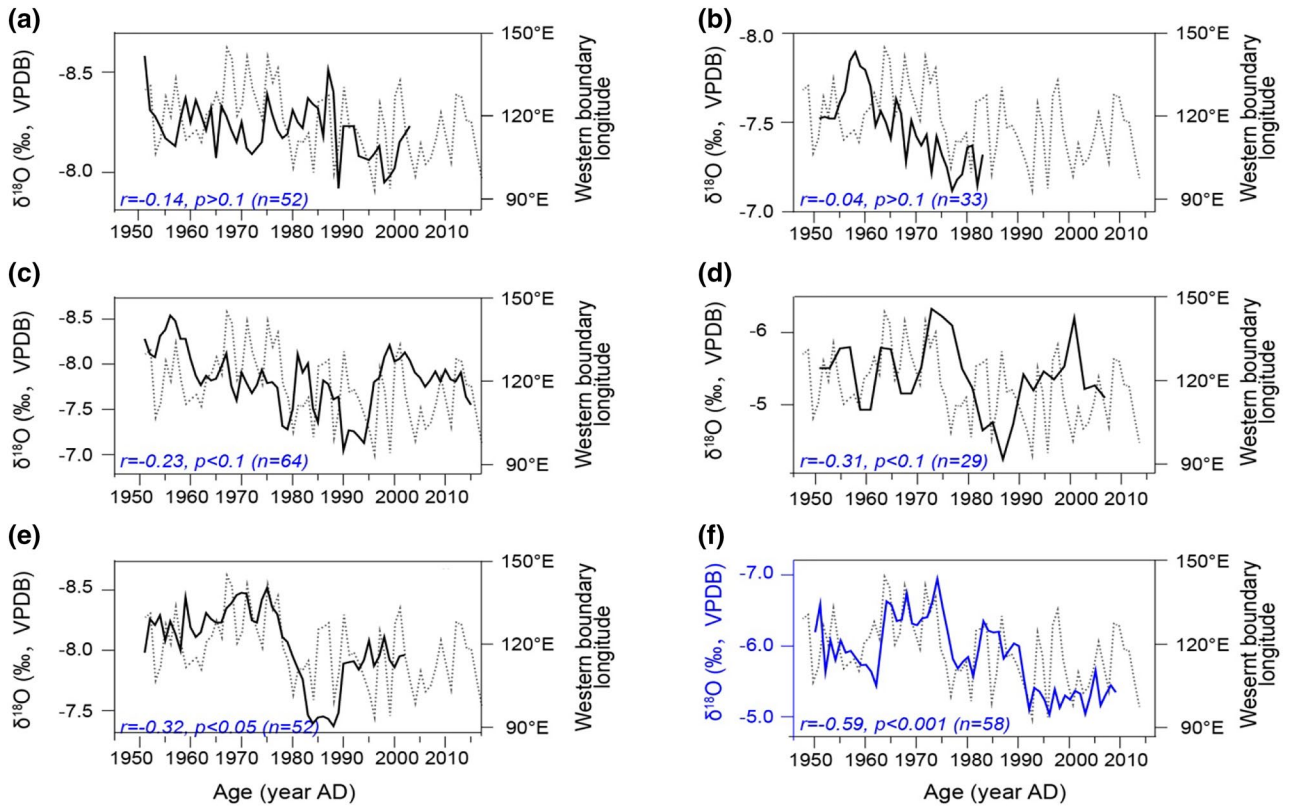

Fig. 5 Comparison between changes of the WPSH western boundary and Chinese cave $\delta^{18}O$ records. Dotted curves represent the longitudes in variations of the WPSH western boundary (from NCCC data). Dark curves represent records from Wanxiang (**a**) (Zhang et al. 2008), Dongge (**b**) (Zhao et al. 2015), Shihua (**c**) (Li et al. 2017), Yuhua (**d**) (Jiang et al. 2012) and Heshang (**e**) (Hu et al. 2008) caves. The blue curve represents the record from Xianglong Cave (**f**) (Tan et al. 2016). Cave data were interpolated to 1–2 years in order to compare with WPSH data except for Shihua and Xianglong records that already have seasonal resolutions. Correlation coefficients (r) are shown in each plot. The correlation coefficient value for the Shihua record is 0.21 and 0.23 using the interpolating data and annual-average data, respectively, and for the Xianglong record, $r = 0.52$ and 0.59, respectively. The cave records without significant correlations with the WPSH are not shown, including Xiaobailong (Tan et al. 2016) ($r = 0.33$, $p > 0.1$, n = 15), Huangye (Tan et al. 2011) ($r = -0.07$, $p > 0.1$, n = 33) and Wuya (Tan et al. 2014) ($r = -0.21$, $p > 0.1$, n = 45)

structure' (e.g., Tao and Chen 1987; Gong and Ho 2002; Ding et al. 2008; He et al. 2017).

On the basis of the analysis of moisture fluxes derived from the Pacific and Indian Oceans (Cao et al. 2012, 2016; Tan 2009, 2011, 2013, 2016; Cao pers. comm.), cave $\delta^{18}O$ records from coastal regions of southeastern China (such as Yuhua Cave) may be dominantly controlled by the proximal Pacific/South China Sea moisture with little contribution from the moisture derived from the Indian Ocean. In contrast, $\delta^{18}O$ records from western China, such as Xiaobailong, are dominantly controlled by moisture from the remote Indian Ocean (Cai et al. 2015). In addition, the apparent 'amount effect' as mentioned above may sensitively affect Wanxiang, Wuya, Huangye and likely Shihua $\delta^{18}O$ records, and overwhelm the 'circulation effect' that is presumably diminished due to their geographic locations with less or negligible contributions from the Pacific moisture sources (Fig. 1). Notably, these sites are located along the summer monsoon fringe with lower annual precipitation, and thus large variations in summer rainfall amount in the areas can significantly bias the mean annual $\delta^{18}O$ value accordingly. Indeed, the $\delta^{18}O$ records from Wanxiang (Zhang et al. 2008), Wuya (Tan et al. 2014), Yuhua (Jiang et al. 2012), Huangye (Tan et al. 2011), Xiaobailong (Tan et al. 2016) and Shihua (Li et al. 2017) cave show a significant anti-correlation with local annual precipitation amount, and/or summer precipitation amount, as well as the dry/wet index established in the corresponding areas.

5.2 Influence of the WPSH on precipitation $\delta^{18}O$: cave monitoring results

Associated with the intensity change, the WPSH western boundary shifted dramatically from 2010 to 2011 from

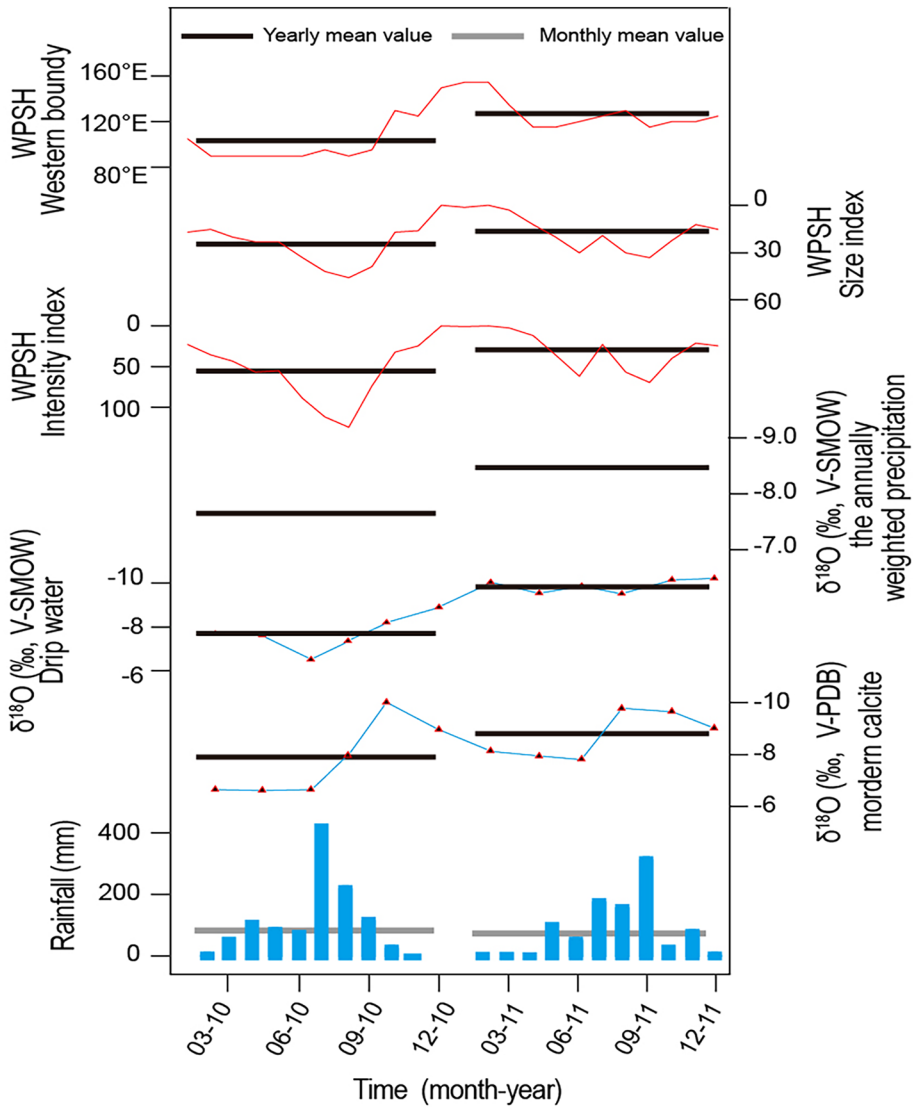

Fig. 6 Comparison of the WPSH index and cave monitoring records in 2010 and 2011. Horizontal lines show annual average values. The plots from the top to bottom are the WPSH western boundary index, the WPSH size index, the WPSH intensity index (the WPSH data from NCCC) (e.g., Zhao 1999; Zhou et al. 2009), the annually weighted precipitation $\delta^{18}O$ at the study area, drip water $\delta^{18}O$ and calcite $\delta^{18}O$ from the monitoring cave, and rainfall at the study area, respectively (the cave monitoring data from Zhao et al. 2014; Sun 2017)

103.3°E to 127.5°E, the second largest abrupt shift observed during the last 20 years (after the largest one from 1998 to 1999). Our Jiguan Cave monitoring results show that $\delta^{18}O$ values of dripwater and modern calcite changed accordingly (Fig. 6). Annual precipitations changed from ~1130 to ~950 mm from 2010 to 2011, whereas the weighted annual $\delta^{18}O$ values change from −7.6 to −8.5‰ (Fig. 6). These data show an opposite change as expected by the 'amount effect', which supports our interpretation that the 'circulation effect' is dominant at this site while the 'amount effect' is suppressed (Zhao et al. 2014; Sun 2017).

In order to further explore the $\delta^{18}O$ change, we analyzed the water vapor flux of the atmosphere in 2010 and 2011(Fig. 7b, c). The water vapor flux chart shows that the atmospheric circulation system that drives the Pacific water vapor in summer moved considerably westward in 2010, bringing more moisture enriched in ^{18}O from proximal oceans into the study area (Tan 2009, 2011, 2013, 2016), as compared to 2011. This change is consistent with the local precipitation $\delta^{18}O$ data that record a weighted annual precipitation $\delta^{18}O$ value of −7.6‰ in 2010, significantly higher than in 2011 (−8.5‰). Similarly, cave monitoring data also show that $\delta^{18}O$ values of dripwater and modern calcite are higher in 2010 than in 2011 (Fig. 6).

5.3 Reconstructing the WPSH variability

Our analyses show clearly that the DSY $\delta^{18}O$ record does not have a significant correlation with the mean annual precipitation amount ($r=0.13$, $p>0.1$) or 'amount effect' (Fig. 8a), and instead, it highly correlates with variations in the mean annual WPSH size ($r=0.37$, $p<0.05$), intensity ($r=0.42$, $p<0.01$) and the location of the western boundary ($r=-0.46$, $p<0.001$) (Fig. 8c), as well as the WPSH variations in winter ($r=-0.58$, $p<0.001$) and summer ($r=-0.43$, $p<0.001$) half year (Fig. 8b).

Our data shows that DSY and XL records correlate significantly ($r=0.4$, $p<0.001$), and both correlate significantly with the position of the western boundary of the WPSH ($r=-0.46$ and -0.59, respectively with $p<0.001$). This

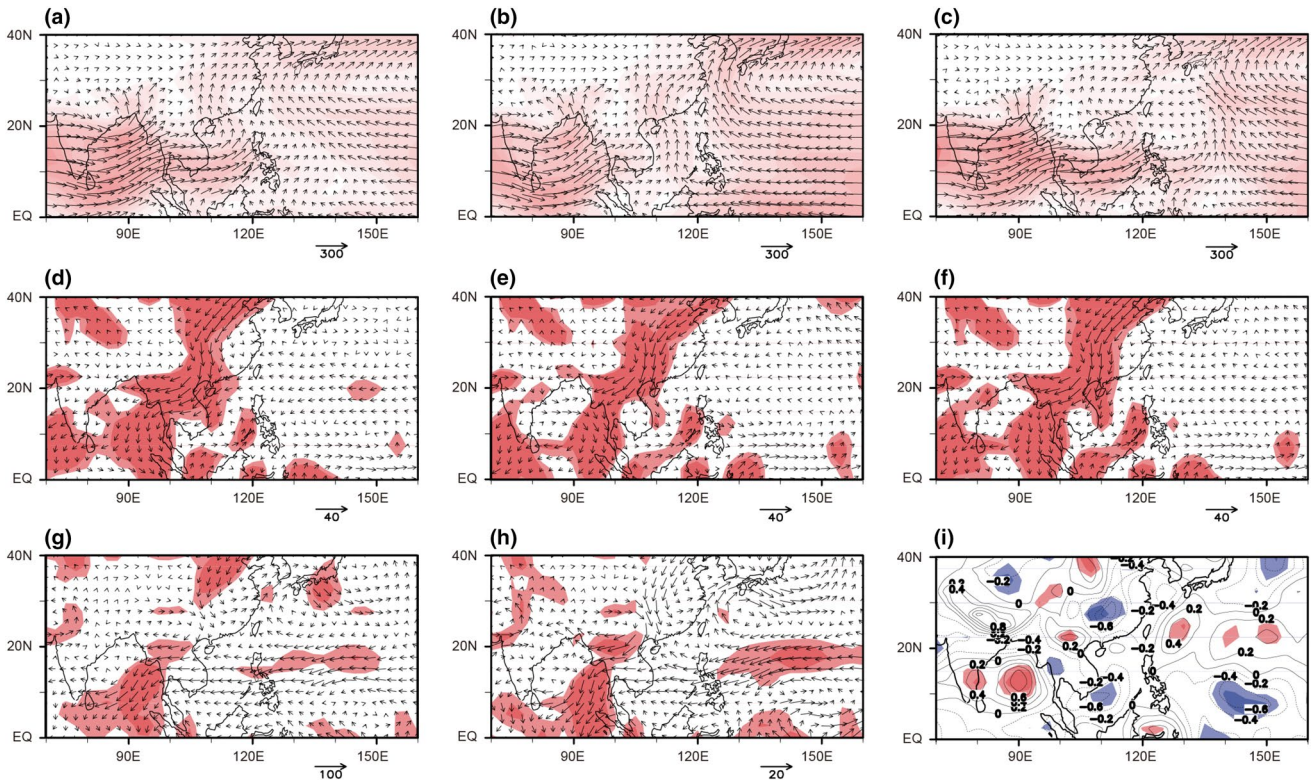

Fig. 7 Moisture fluxes (kg m^{-1} s^{-1}) integrated from 1000 to 300 hPa during the main rainy season (July–September) in 1948–2016 average (**a**), in 2010 (**b**) and in 2011 (**c**), respectively. Their anomalies (kg m^{-1} s^{-1}) associated with the $\delta^{18}O$ of DSY (**d**) and XL (**e**) records, the new reconstructed WPSH western boundary indexes (**f**) and the NCCC WPSH western boundary longitude (*-1) (**h**). The difference of the column-integrated water vapor flux averages between the 10 WPSH westward-anomaly years and the 10 WPSH eastward-anomaly years (**g**). The water vapor flux divergence anomalies associated with the NCCC WPSH western boundary longitude (*-1) (**i**). The water vapor flux amount is depicted by color (increase with darkness) (**a**–**c**), which is consistent with the vector change. Total atmospheric water vapor fluxes are from monthly reanalysis data from the NCEP and NCAR. The areas passing the significance test at the 95% and 99% confidence levels are shown by shaded areas with light red and dark red, respectively (**d**–**i**)

implies that the westward extent of the WPSH would bring in more (less) moisture from the Pacific/South China Sea (the Indian Ocean) source, resulting in heavier (lighter) $\delta^{18}O$ of precipitation in DSY and XL cave sites, and vice versa. Further analyses show that the column-integrated water vapor fluxes regressed respectively onto the DSY (Fig. 7d), XL (Fig. 7e) and the variance of the WPSH western boundary (Fig. 7h, derived from NCCC data), exhibit a similar anomalous pattern with significantly reduce of southwest water vapor fluxes from the Indian Ocean into the EASM region. Furthermore, using the NCCC WPSH western boundary data with a criterion of 1 standard deviation, we identified 10 years (1979, 1983, 1987, 1994, 1995, 1998, 2003, 2005, 2010 and 2016) when the WPSH extended significantly westward and other 10 years (1952, 1957, 1967, 1968, 1971, 1974, 1975, 1976, 1989 and 2000) when the WPSH retreated significantly eastward. The difference of the column-integrated water vapor fluxes between the 10 year averages when the WPSH extended westward and retreated eastward (Fig. 7g) also demonstrates a similar pattern with largely reduced southwest water vapor fluxes from the Indian Ocean into the EASM region.

The strong correlation of DSY and XL records with the WPSH and their conceivable causal linkage allow us to establish a new WPSH index using the cave records. Our WPSH index is constructed by the average of normalized DSY and XL records for the time period of 1908–2009, and the normalized DSY data for 1907–1812 (Fig. 9). The new WPSH index correlates significantly to the annual (as well as seasonal) variability of the WPSH western boundary ($r = 0.61$, $p < 0.001$) (Figs. 9, 10). This reconstruction extends the WPSH variation history further back in time from the last ~ 60 to 200 years. Our WPSH index manifests a 200-year long-term decrease trend with a dramatic weakening after 1970s, which is akin to the variance of the large-scale Indo-Pacific sea level pressure gradient index (ΔSLP, Vecchi et al. 2006) (Fig. 9). A suite of global climate model simulations revealed that the decrease trend of the ΔSLP can be linked to the weakening of the tropical Pacific circulation or the Walker Circulation (Vecchi et al.

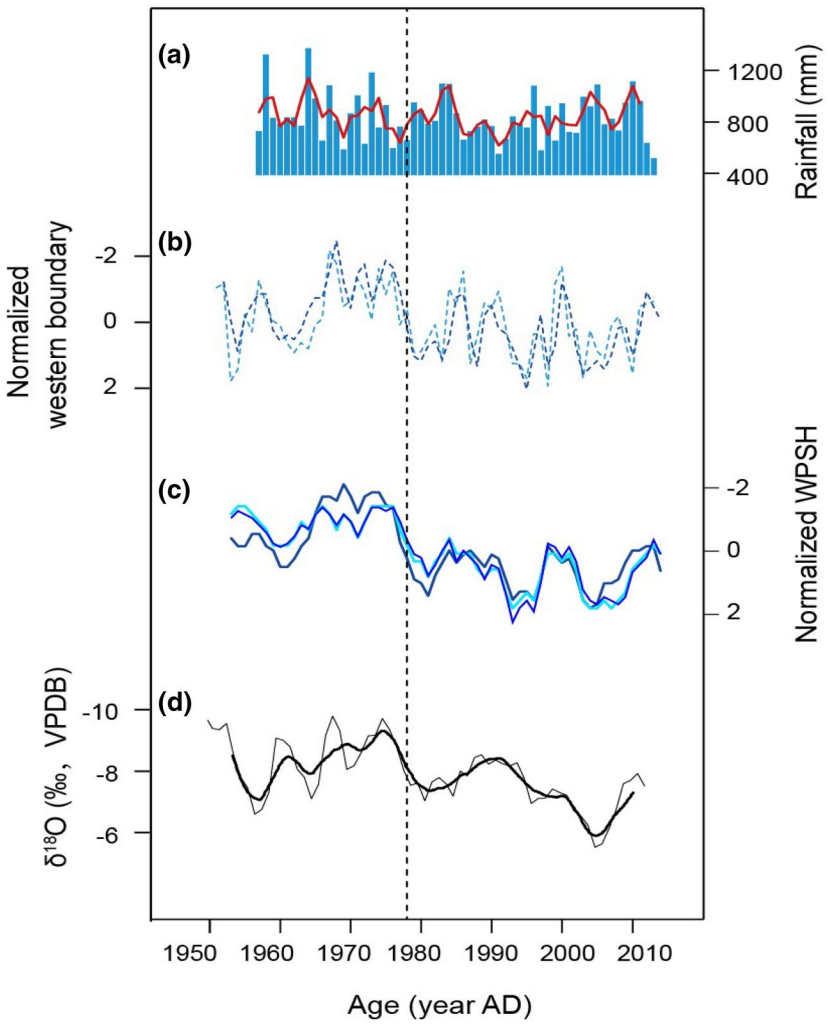

Fig. 8 Comparison between Luanchuan annual precipitation, normalized WPSH indexes and DSY1201 $\delta^{18}O$ record. **a** The Luanchuan annual precipitation (blue bars) and 5 years running average (red line). **b** The normalized WPSH western boundaries in May–October (dotted light blue line) and November–April (next year) (dotted dark blue line). **c** The 5 years running averages of the normalized WPSH western boundary (dark blue line), size (light blue line) and intensity indexes (blue line) (the WPSH data from NCCC: http://cmdp.ncc-cma.net/Monitoring/cn_index_130.php) (e.g., Zhao 1999; Zhou et al. 2009). **d** The DSY1201 $\delta^{18}O$ record, interpolated to 1 year resolution for the comparison with the WPSH index, and the 5-year running averages of it (thick black lines)

2006). Thus the observed covariance of the WPSH with the ΔSLP implies that the tropical Pacific circulation or the Walker Circulation changes may have dominated the long-term variation of the WPSH. Intriguingly, in the same climate models (Vecchi et al. 2006), the tropical Pacific circulation trend was largely attributed to the global surface warming or anthropogenic forcing (Held and Soden 2006). Indeed, our WPSH index shows a clear anomaly after the ~1980s in the context of the last 200-year variations (Fig. 9b), which coincides with the global surface temperature anomaly (Fig. 9c) (e.g., Li et al. 2012; IPCC 2014).

5.4 The interdecadal oscillation of the WPSH

The interdecadal variability of the WPSH have received few attentions, in comparison with its 2–7 year periodicity (Hu 1997; Sun et al. 2017), and the mechanism behind remains unclear (Wang et al. 2013). Our high-resolution reconstruction of the WPSH extends the 60-year instrumental record further back to the last 200 years (Figs. 10, 11), providing a new insight into the interdecadal–interannual variability of the WPSH. Our data show persistent ~12 and 2–7 year periodicities (Fig. 12a) over the last 200 years, which agrees with periodicities observed from the WPSH western boundary, intensity and size data over the last ~60 years (Fig. 12b–d), but more robust. Clearly, these two periodicities correspond respectively to one of major solar radiation cycles (~12 years) and the El Niño–Southern Oscillation (ENSO) periodicity (2–7 years) (Fig. 12). Moreover, our analyses also show that the WPSH index correlate significantly to both the solar radiation ($r=0.56$, $p<0.001$) (Lean et al. 1995) and the Southern Oscillation Index (SOI) ($r=0.22$, $p<0.05$) (Fig. 11). In addition, as paced presumably by the persistent 12-year periodicity, the WPSH has intensified and shifted westward since 2015 (data source: http://cmdp.ncc.cma.gov.cn/cn/monitoring.htm), consistent with the sunspot maximum in 2014 (data source: https://solarscience.msfc.nasa.gov/predict.shtml) (Fig. 12).

The dynamic how solar irradiance modulates the Earth's climate, such as monsoons and the WPSH variability, remains a complex issue (Gray et al. 2010; Van et al. 2004;

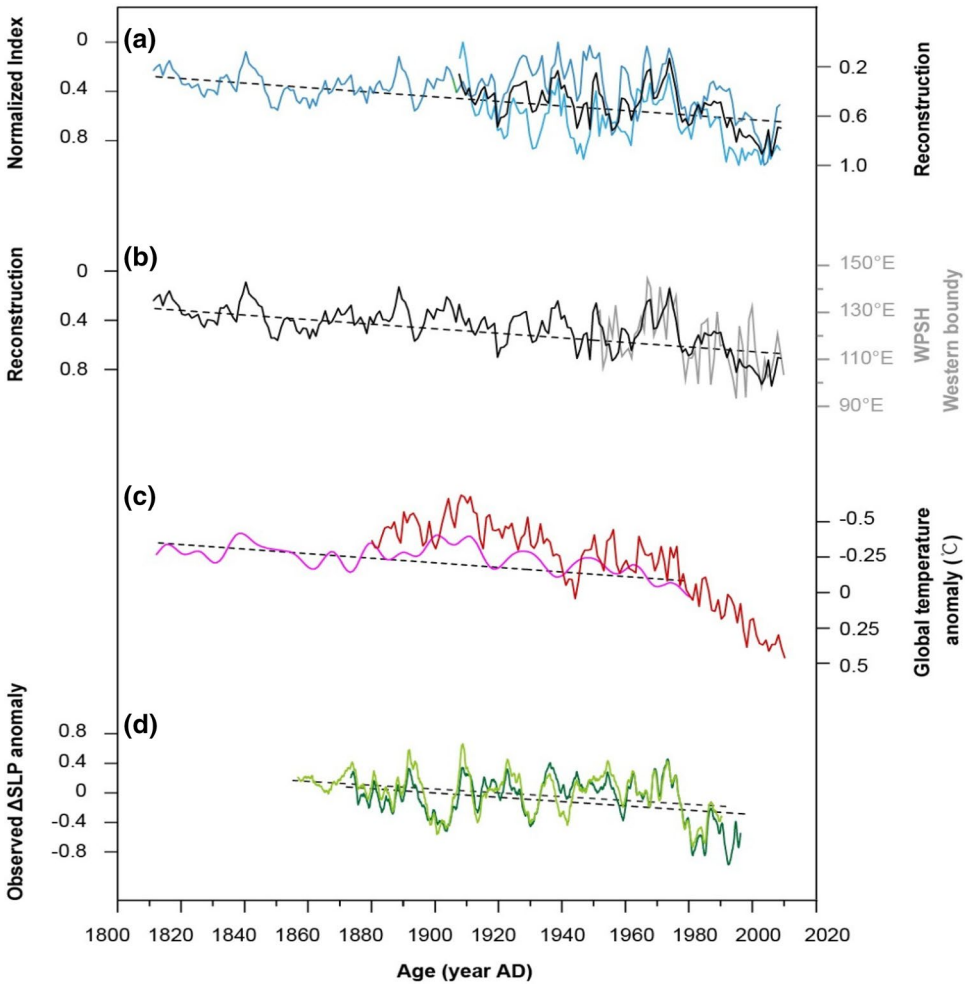

Fig. 9 Reconstructed index of the WPSH western boundary and comparison with the global temperature anomalies and the Indo-Pacific sea level pressure gradient index (ΔSLP). **a** Normalized DSY (dark blue) and XL (light blue) $\delta^{18}O$ records and their average (black). **b** Reconstructed (black line, this study) and original (gray line, data from NCCC) WPSH western boundary records. **c** The Global temperature anomaly in 1812–2009 (the purple line in 18,121,980 from Mann and Jones 2003; the red line in 18,702,009 from the National Oceanic for Atmospheric Administration, https://www.ncdc.noaa.gov/data-access/marineocean-data). **d** The 5-years running average of the ΔSLP (Vecchi et al. 2006). The data are from observation (light green) and Hadley Centre (dark green) respectively (Basnett and Parker 1997; Kaplan et al. 2000). The dotted lines show the decrease trend

Meehl et al. 2009; White and Liu 2008). A number of studies (e.g., White et al. 1997; Meehl et al. 2009; Gray et al. 2010) have found clear evidences of the 9–13 year solar cycle signal in sea surface temperature (SST) records globally, whereas the SST of the Indian, Pacific and Atlantic oceans have been noted to have remarkably local or remote effects on the WPSH strengthening (e.g., Nitta 1987; Huang and Li 1989; Wang et al. 2000, 2013; Xie et al. 2009; Yang et al. 2007; Zhou et al. 2009; He and Zhou 2014, 2015a, b; He et al. 2017; Hong et al. 2014). It thus appears that the solar irradiation change can affect the WPSH variability via a positive atmosphere–ocean feedback. However, controversies in the WPSH formation endures (e.g., Ye and Gao 1979; Ye and Wu 1998; Hoskins 1996; Huang et al. 2016; He et al. 2015), and more observational and modeling studies are critically needed.

5.5 Possible physical processes of the WPSH

During the past two decades, a large number of researches have been focused on the physical processes of the WPSH variations, bringing up various propositions. A mechanism so-called 'Kelvin-wave-induced Ekman divergence' was proposed to explain the WPSH dynamics, which invokes SST over the tropical Indian Ocean and tropical West Pacific Ocean (e.g., Wang et al. 2000, 2013; Xie et al. 2009; Wu et al. 2010; He and Zhou 2014, 2015a, b; Hong et al. 2014). Our WPSH reconstruction appears to correlate with the tropical SST anomaly (SSTA) in the West Pacific Ocean ($r=0.57$, $p<0.001$) and tropical Indian Oceans ($r=0.56$, $p<0.001$) (Tierney et al. 2015) (Fig. 11). Recently, the warm tropical Atlantic SST mode was considered to be able to enhance the WPSH and shift it westward (Hong et al. 2014). In addition, Sun et al. (2017) also suggested that the tropical Atlantic SST acts as a key pacemaker of the western Pacific decadal climate variability. Our WPSH reconstruction also correlates with the tropical SSTA in the tropical Atlantic (Tierney et al. 2015) ($r=0.44$, $p<0.001$) (Fig. 11), in line with the interpretations.

On the other hand, the condensation heating released by AM rainfall was viewed as an important feedback affecting the WPSH (Hoskins 1996; Liu et al. 2001; Wu and Liu 2003; Wu et al. 2004, 2009; He and Zhou 2014, 2015a, b; Chowdary et al. 2010; Xie et al. 2009). This is consistent with many observations that show the wet anomalies in the AM region occurred in accordance with WPSH intensifications (Gong and Ho 2002; Chowdary et al. 2010). Our WPSH index also shows a significant correlation with rainfall anomaly in southern China ($r=0.21$, $p<0.001$) (Fig. 11). In addition, during the peak years

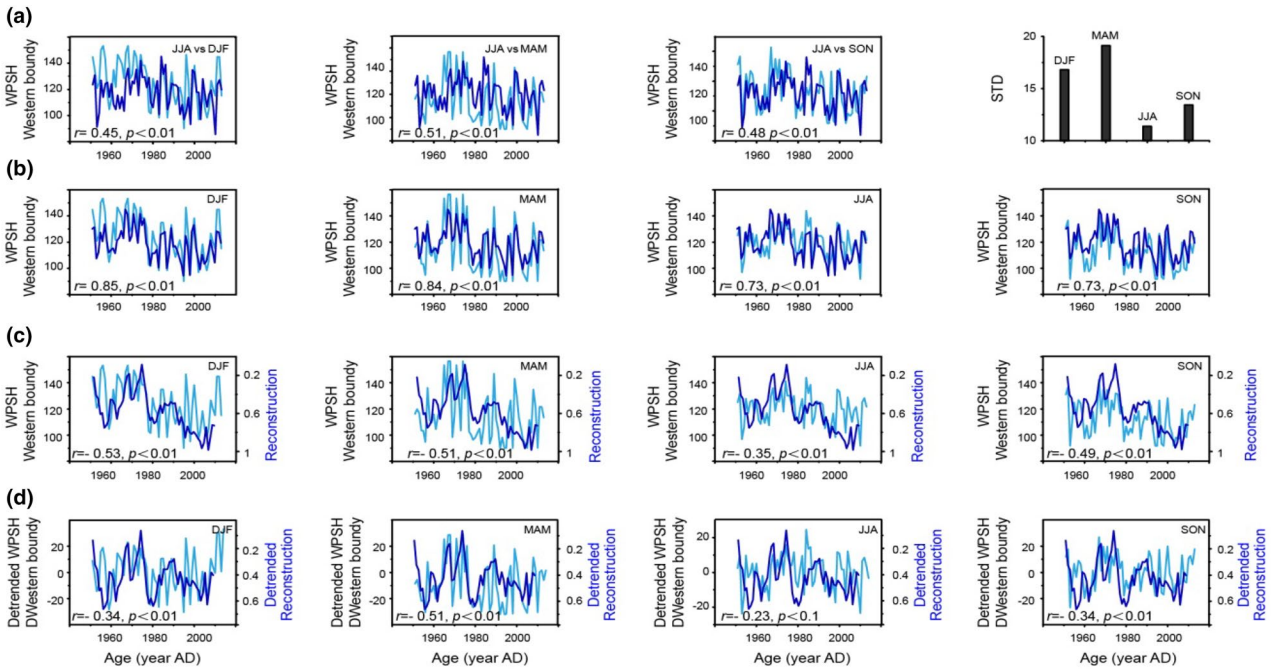

Fig. 10 Seasonal variability of the WPSH western boundary. **a** The NCCC WPSH western boundary variability in summer (dark blue) in comparison with those in other seasons (light blue), and the standard deviations (STD) of those in different seasons (the right plot). **b** The variability of the mean annual WPSH western boundary (dark blue) in comparison with the seasonal variations (light blue) (data from NCCC). **c** The variability of the reconstructed WPSH western boundary index (dark blue) in comparison with seasonal NCCC WPSH western boundary variations (light blue). **d** The detrended reconstructed WPSH index (dark blue) in comparison with detrended seasonal NCCC WPSH western boundary variations (light blue)

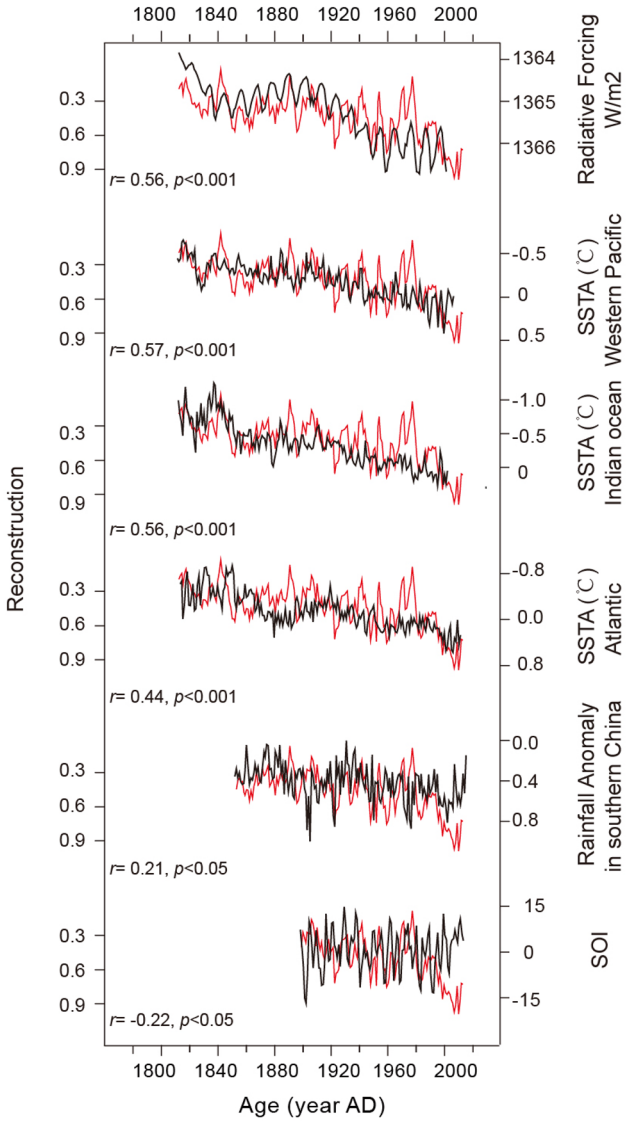

Fig. 11 Comparison of the reconstructed WPSH western boundary index with other climate records. Red curve is the constructed index (this study). Black curves from top to bottom are solar radiation (Lean et al. 1995), three different tropical SSTA (Tierney et al. 2015), southern rainfall anomalies in the region of 21°N–30°N and 104°E–120°E (http://climexp.knmi.nl/select.cgi), Southern Oscillation Index (SOI) over in the last 100 years (1908–2009) (https://crudata.uea.ac.uk/cru/data/pci.htm)

of solar irradiation, regions with enhanced precipitation extends from the ISM domain to the West Pacific Warm Pool (Van et al. 2004), coincided with AM rainfall anomalies (~20% above normal) (Van and Meehl 2012). This thermal–hydrological mode intensifies the WPSH via the mechanism of a positive atmosphere–ocean feedback (Wang et al. 2000, 2013; Xie et al. 2009; Yang et al. 2007; Zhou et al. 2009; He and Zhou 2014, 2015a, b; He et al. 2017) and/or the energy dispersion (Nitta 1987; Huang and Li 1989) between the WPSH and the Indo-Pacific Oceans (Wu and Liu 2003; Wu et al. 2004; Liu et al. 2001; Lu and Dong 2001; Cao et al. 2009, 2012, 2016). In sum, the propositions of the tropical SST patterns and AM rainfall feedback may explain at least some important aspects of the physical process of the WPSH, but more modeling and observational studies are critical to further assess the role of the SST and AM rainfall feedback in amending the WPSH.

6 Conclusions

The major factors controlling the $\delta^{18}O$ of precipitation and speleothem calcite on seasonal to multidecadal timescales vary within the EASM region of eastern China. The Qinling region in central China is unique and more sensitive to variations in the position of the western boundary of the WPSH, which in turn regulates the alteration of moisture sources from the proximal Pacific Ocean and remote Indian Ocean, consistent with the 'circulation effect'. On the other hand, cave sites in other monsoon regions of China with dominant moisture sources from either the Pacific or the Indian Ocean are not significantly correlated with WPSH variations. For instance, cave records close to the summer monsoon fringe and near the coast of southeastern China show the evidence of the apparent 'amount effect'.

On the basis of the high-resolution DSY and XL cave records and their strong correlations with the variations of the WPSH western boundary, we extended the WPSH variation history from instrumental records over the last ~60 years further back in time to the last 200 years by constructing a new WPSH index to indicate changes in the WPSH western boundary. Our WPSH index shows a long-term decrease over the last 200 years with a dramatic decline since 1980s which may be linked to the tropical atmospheric circulation weakening and/or anthropogenic forcing. The WPSH variations also show two distinct periodicities, 12 and 2–7 years respectively, that can be causally linked to the solar and ENSO variances correspondingly. Our work demonstrates that the cave record can potentially extend the high-resolution WPSH variation history much longer than instrumental records, which opens the door to a more precise and robust understanding of the climate dynamics behind. In particular, the climate changes, including the WPSH variability, were closely linked to both natural and anthropogenic forcing. In this regard, the critical observation was not our WPSH reconstruction over the last ~60 years, which is also observed in various instrumental records, but rather the variability at earlier times and their relations with other regional–global climate changes. The reconstructed WPSH records establish the characters of natural climate change beyond instrumental records, merely from which

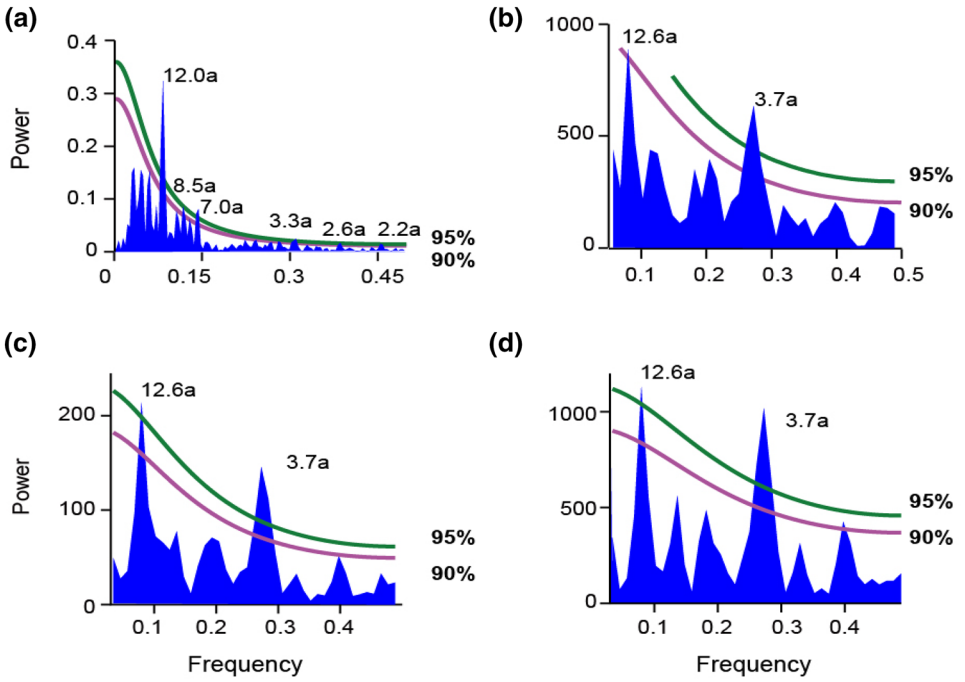

Fig. 12 Spectral analysis results. **a** Power spectral analysis result of the new reconstructed WPSH index detrended by Singular Spectrum Analysis (Elsner and Tsonis 2013). **b, c** and **d** Power spectral analysis results of the NCCC WPSH western boundary, the WPSH size and intensity index in 1951–2016

we may distinguish the trends and periodicities observed in the last ~ 60 years as clear anomalies or persistent natural variations.

Acknowledgements We thank Jie Cao of School of Resource Environment and Earth Science, University of Yunnan, for his constructive comments and thank Tingyong Li of School of Geography Sciences, Southwest University, and Xiuyang Jiang, College of Geography Sciences, Fujian Normal University, for sharing their stalagmite $\delta^{18}O$ data. This study was supported by the National Natural Science Foundation of China (NSFC) (41731174, 41672160, 41761144069 and 41561144003) and US NSF Grants 1702816. We would also like to thank three anonymous reviewers for their constructive comments.

References

Basnett T, Parker D (1997) Development of the global mean sea level pressure data set GMSLP2 (Climate Research Technical Note 79. Hadley Centre, Met Office, Exeter

Cai BG, Edwards RL, Cheng H, Tan M, Wang XJ, Liu T (2008) A dry episode during the Younger Dryas and centennial-scale weak monsoon events during the early Holocene: a high-resolution stalagmite record from southeast of the Loess Plateau, China. Geophys Res Lett 35(2):2705

Cai YJ, Fung IY, Edwards RL, An ZS, Cheng H, Lee JE, Tan LC, Shen CC, Wang XF, Day JA, Zhou WJ, Kelly MJ, Chiang CH (2015) Variability of stalagmite-inferred Indian monsoon precipitation over the past 252,000 y. Proc Natl Academy Sci, 112(10):2954–2959

Caley T, Roche DM, Renssen H (2014) Orbital Asian summer monsoon dynamics revealed using an isotope-enabled global climate model. Nat Commun 5:5371

Cao J, Yang RW, You YL, Huang W (2009) The mechanism for the impact of sea surface temperature anomaly on the ridgeline surface of Western Pacific. Sci China 52(11):1864

Cao J, Hu J, Tao Y (2012) An index for the interface between the Indian summer monsoon and the East Asian summer monsoon. J Geophys Res Atmos 117(18):108

Cao J, Gui S, Su Q, Yang Y (2016) The variability of the Indian–East Asian Summer Monsoon interface in relation to the Spring Seesaw Mode between the Indian Ocean and the Central-Western Pacific. J Clim 29(13):5027–5040

Chen ST, Wang YJ, Cheng H, Lawrence ER, Wang XF, Kong XG, Liu DB (2016) Strong coupling of asian monsoon and antarctic climates on sub-orbital timescales. Sci Rep 6:32995

Cheng H, Edwards RL, Hoff J, Gallup CD, Richards DA, Asmerom Y (2000) The half-lives of uranium-234 and thorium-230. Chem Geol 169(1):17–33

Cheng H, Edwards RL, Wang YJ, Kong XG, Ming YF, Kelly MJ, Wang XF, Gallup CD, Liu WG (2006) A penultimate glacial monsoon record from Hulu Cave and two-phase glacial terminations. Geology 34(3):217–220

Cheng H, Edwards RL, Broecker WS, Denton GH, Kong XG, Wang YJ, Zhang R, Wang XF (2009a) Ice age terminations. Science 326:248–252

Cheng H, Fleitmann D, Edwards RL, Wang XF, Cruz FW, Auler AS, Mangini A, Wang YJ, Kong XG, Burns SJ, Matter A (2009b) Timing and structure of the 8.2 kyr BP event inferred from $\delta^{18}O$ records of stalagmites from China, Oman, and Brazil. Geology 37(11):1007–1010

Cheng H, Sinha A, Wang X, Cruz FW, Edwards RL (2012) The Global Paleomonsoon as seen through speleothem records from Asia and the Americas. Clim Dyn 39(5):1045–1062

Cheng H, Edwards RL, Shen CC, Polyak VJ, Asmerom Y, Woodhead J, Hellstrom J, Wang YJ, Kong XG, Spötl C, Wang XF, Alexander EC (2013) Improvements in ^{230}Th dating, ^{230}Th and ^{234}U half-life values, and U–Th isotopic measurements by multi-collector inductively coupled plasma mass spectrometry. Earth Planet Sci Lett 371:82–91

Cheng H, Edwards RL, Sinha A, Spötl C, Yi L, Chen ST, Kelly M, Kathayat G, Wang XF, Li XL, Kong XG, Wang YJ, Ning YF, Zhang HW (2016) The Asian monsoon over the past 640,000 years and ice age terminations. Nature 534:640–646

Chowdary JS, Xie SP, Lee JY, Yu K, Wang B (2010) Predictability of summer northwest Pacific climate in 11 coupled model hindcasts: local and remote forcing. J Geophys Res Atmos (1984–2012) 2010:1842–1851

Clemens SC, Prell WL, Sun Y (2010) Orbital-scale timing and mechanisms driving Late Pleistocene Indo-Asian summer monsoons: reinterpreting cave speleothem $\delta^{18}O$. Paleoceanography 25(4):4207

Dansgaard W (1964) Stable isotopes in precipitation. Tellus 16(4):436–468

Dayem KE, Molnar P, Battisti DS, Roe GH (2010) Lessons learned from oxygen isotopes in modern precipitation applied to interpretation of speleothem records of paleoclimate from eastern Asia. Earth Planet Sci Lett 295(1):219–230

Ding YH, Wang Z, Sun Y (2008) Inter-decadal variation of the summer precipitation in East China and its association with decreasing Asian summer monsoon. Part I: Observed evidences. Int J Climatol 28(9):1139–1161

Dorale JA, Liu Z (2009) Limitations of Hendy test criteria in judging the paleoclimatic suitability of speleothems and the need for replication. J Cave Karst Stud 71(1):73–80

Duan WH, Ruan JY, Luo WJ, Li TY, Tian LJ, Zeng GN, Zhang DZ, Bai YJ, Li JL, Tao T, Zhang PZ, Baker A, Tan M (2016) The transfer of seasonal isotopic variability between precipitation and drip water at eight caves in the monsoon regions of china. Geochim Cosmochim Acta 183:250–266

Edwards RL (1988) High precision thorium-230 ages of corals and the timing of sea level fluctuations in the late Quaternary. PhD Thesis, California Institute of Technology

Edwards RL, Chen JH, Wasserburg GJ (1987) $^{238}U^{234}U^{230}Th^{232}Th$ systematics and the precise measurement of time over the past 500,000 years. Earth Planet Sci Lett 81(2–3):175–192

Elsner JB, Tsonis AA (2013) Singular spectrum analysis: a new tool in time series analysis. Springer, Berlin

Fleitmann D, Burns SJ, Mudelsee M, Neff U, Kramers J, Mangini A, Matter A (2003) Holocene forcing of the Indian monsoon recorded in a stalagmite from southern Oman. Science 300:1737–1739

Frisia S, Borsato A, Fairchild IJ, McDermott F (2000) Calcite fabrics, growth mechanisms, and environments of formation in speleothems from the Italian Alps and southwestern Ireland. J Sedim Res 70(5):1183–11196

Genty D, Quinif Y (1996) Annually laminated sequences in the internal structure of some Belgian stalagmites—importance for paleoclimatology. J Sedim Res 66(1):275–288

Goldsmith Y, Broecker WS, Xu H, Polissar PJ, Demenocal PB, Porat N, Lan JH, Cheng P, Zhou WJ, An ZS (2017) Northward extent of East Asian monsoon covaries with intensity on orbital and millennial timescales. Proc Natl Acad Sci USA 114(8):1817–1821

Gong DY, Ho CH (2002) Shift in the summer rainfall over the Yangtze River valley in the late 1970s. Geophys Res Lett 29(10):71–78

Gray LJ, Beer J, Geller M, Haigh JD, Lockwood M, Matthes K, Cubasch U, Fleitmann D, Harrison G, Hood L, Luterbacher J, Meehl GA, Shindell D, Geel B, White W (2010) Solar influences on climate. Rev Geophys 48(4):1032–1047

He C, Zhou T (2014) The two interannual variability modes of the Western North Pacific Subtropical High simulated by 28 CMIP5–AMIP models. Clim Dyn 43(9–10):2455–2469

He C, Zhou T (2015a) Responses of the Western North Pacific Subtropical High to global warming under RCP4.5 and RCP8.5 scenarios projected by 33 CMIP5 models: the dominance of tropical Indian ocean-tropical western Pacific SST gradient. J Clim 28(1):365–380

He C, Zhou T (2015b) Decadal change of the connection between summer western North Pacific Subtropical High and tropical SST in the early 1990s. Atmos Sci Lett 16(3):253–259

He C, Zhou T, Lin A, Wu B, Gu D, Li C, Zheng B (2015) Enhanced or weakened western north Pacific subtropical high under global warming? Sci Rep 5:16771

He C, Lin A, Gu D, Li C, Zheng B, Zhou T (2017) Interannual variability of eastern China summer rainfall: the origins of the meridional triple and dipole modes. Clim Dyn 48(1–2):683–696

Held IM, Soden BJ (2006) Robust responses of the hydrological cycle to global warming. J Clim 19(21):5686–5699

Hendy CH (1971) The isotopic geochemistry of speleothems—I. The calculation of the effects of different modes of formation on the isotopic composition of speleothems and their applicability as palaeoclimatic indicators. Geochim Cosmochim Acta 35(8):801–824

Hong CC, Chang TC, Hsu HH (2014) Enhanced relationship between the tropical Atlantic SST and the summertime western north Pacific subtropical high after the early 1980s. J Geophys Res Atmos 119(7):3715–3722

Hoskins BJ (1996) On the existence and strength of the summer subtropical anticyclones. Bull Am Meteorol Soc 77:1287–1292

Hu ZZ (1997) Interdecadal variability of summer climate over East Asia and its association with 500 hPa height and global sea surface temperature. J Geophys Res Atmos 102(D16):19403–19412

Hu CY, Henderson GM, Huang JH, Xie SC, Sun Y, Johnson KR (2008) Quantification of Holocene Asian monsoon rainfall from spatially separated cave records. Earth Planet Sci Lett 266(3):221–232

Huang RH, Li L (1989) Numerical simulation of the relationship between the anomaly of subtropical high over East Asia and the convective activities in the western tropical Pacific. Adv Atmos Sci 6(2):202–214

Huang YY, Li XF, Wang HJ (2016) Will the Western Pacific Subtropical High constantly intensify in the future? Clim Dyn 47(1–2):567–577

IPCC (2014) Climate change 2014 synthesis report, summary for policymakers. Environ Policy Collect 27(2):408

Jiang XY, Li ZZ, Li JQ, Kong XG, Guo Y (2012) Stalagmite $\delta^{18}O$ record from Yuhua Cave over the past 500 years and its regional climate significance. Sci Geogr Sin 32:207–212

Jiang XY, Wang X, He Y, Hu HM, Li Z, Spötl C, Shen CC (2016) Precisely dated multidecadally resolved Asian summer monsoon dynamics 113.5–86.6 thousand years ago. Quat Sci Rev 143:1–12

Kaplan A, Kushnir Y Cane MA (2000) Reduced space optimal interpolation of historical marine sea level pressure. J Clim 13:2987–3002

Le Grande A, Schmidt G (2009) Sources of Holocene variability of oxygen isotopes in paleoclimate archives. Clim Past Discuss 5:1133 ~ 1162

Lean J, Beer J, Bradley R (1995) Reconstruction of solar irradiance since 1610: implications for climate change. Geophys Res Lett 22(23):3195–3198

Li WH, Li LF, Ting MF, Liu YM (2012) Intensification of northern hemisphere subtropical highs in a warming climate. Nat Geosci 5(11):830–834

Li XL, Cheng H, Tan LC, Ban FM, Sinha A, Duan WH, Li HY, Zhang HW, Ning YF, Kathtayat G, Edwards RL (2017) The East Asian summer monsoon variability over the last 145 years inferred from the Shihua Cave record, North China. Sci Rep 7:7078

Liu YM, Wu GX, Liu H, Liu P (2001) Condensation heating of the Asian summer monsoon and the subtropical anticyclone in the Eastern Hemisphere. Clim Dyn 17(4):327–338

Liu YH, Henderson GM, Hu CY, Mason AJ, Charnley N, Johnson KR, Xie SC (2013) Links between the East Asian monsoon and

North Atlantic climate during the 8,200 year event. Nat Geosci 6(2):117–120
Lu RY, Dong B (2001) Westward extension of North Pacific subtropical high in summer. J Meteorol Soc Jpn Ser II 79(6):1229–1241
Maher BA (2008) Holocene variability of the East Asian summer monsoon from Chinese cave records: a re-assessment. Holocene 18(6):861–866
Maher BA, Thompson R (2012) Oxygen isotopes from Chinese caves: records not of monsoon rainfall but of circulation regime. J Quat Sci 27(6):615–624
Mann ME, Jones PD (2003) Global surface temperatures over the past two millennia. Geophys Res Lett 30(15):CLM 5–CLM 11
Mattey D, Lowry D, Duffet J, Fisher R, Hodge E, Frisia S (2008) A 53 year seasonally resolved oxygen and carbon isotope record from a modern Gibraltar speleothem: reconstructed drip water and relationship to local precipitation. Earth Planet Sci Lett 269(1):80–95
Meehl GS, Srblaster JM, Matthes K, Sassi F, Van LH (2009) Smplifying the Pacific climate system response to a small 11-year solar cycle forcing. Science 325(5944):1114
Nitta T (1987) Convective activities in the tropical western Pacific and their impact on the northern Hemisphere summer circulation. J Meteorol Soc Jpn 65:373–390
Orland IJ, Edwards RL, Cheng H, Kozdon R, Cross M, Valley JW (2015) Direct measurements of deglacial monsoon strength in a Chinese stalagmite. Geology 43(6):555–558
Pausata FS, Battisti DS, Nisancioglu KH, Bitz CM (2011) Chinese stalagmite δ^8O controlled by changes in the Indian monsoon during a simulated Heinrich event. Nat Geosci 4(7):474–480
Rozanski K, Araguás-Araguás L, Gonfiantini R (1993) Isotope patterns in modern global precipitation, geophysical monograph 78. Clim Change Cont Isot Rec Am Geophys Union Geophys Monogr 78:1–36. https://doi.org/10.1029/GM078p000
Sinha A, Kathayat G, Cheng H, Breitenbach SF, Berkel hammer M, Mudelsee M, Biswas J, Edwards RL (2015) Trends and oscillations in the Indian summer monsoon rainfall over the last two millennia. Nat Commun 6(8):6309
Spötl C, Vennemann TW (2003) Continuous-flow isotope ratio mass spectrometric analysis of carbonate minerals. Rapid Commun Mass Spectrom 17(9):1004–1006
Sun Z (2017) Effects of ENSO circulation conditions on the modern process of oxygen isotope in Karst Cave—an example of Jiguan Cave, Henan Province, China. Master Thesis, Southwest University **(in Chinese with English abstract)**
Sun C, Kucharski F, Li JP, Jin FF, Kang IS, Ding R (2017) Western tropical pacific multidecadal variability forced by the Atlantic multidecadal oscillation. Nat Commun 8:15998
Tan M (2009) Circulation effect: climatic significance of the short term variability of the oxygen isotopes stalagmites form monsoonal China—dialogue between paleoclimate records and modern climate research. Quat Sci 29:851–862 **(in Chinese with English abstract)**
Tan M (2011) Trade-wind driven inverse coupling between stalagmite δ^{18}O from monsoon region of China and large scale temperature. Quat Sci 31(6):1086–1097 **(in Chinese with English abstract)**
Tan M (2013) Circulation effect: response of precipitation δ^{18}O to the ENSO cycle in monsoon regions of China. Clim Dyn 42(3–4):1067–1077
Tan M (2016) Circulation background of climate patterns in the past millennium: uncertainty analysis and re-reconstruction of ENSO-like state. Sci China Earth Sci 59(6):1225–1241
Tan M, Nan SL (2010) Primary investigation on interannual changes in circulation effect of precipitation oxygen isotope in monsoon China. Quat Sci 30(3):620–622 **(in Chinese with English abstract)**
Tan LC, Cai YJ, Cheng H, An ZS, Edwards RL (2009) Summer monsoon precipitation variations in central China over the past 750 years derived from a high-resolution absolute-dated stalagmite. Palaeogeogr Palaeoclimatol Palaeoecol 280(3):432–439
Tan LC, Cai Y, An Z, Edwards RL, Cheng H, Shen CC, Zhang H (2011) Centennial-to decadal-scale monsoon precipitation variability in the semi-humid region, northern China during the last 1860 years: records from stalagmites in Huangye Cave. Holocene 21(2):287–296
Tan LC, An ZS, Huh CA, Cai Y, Shen CC, Shiau LJ, Yan LB, Cheng H, Edwards RL (2014) Cyclic precipitation variation on the western Loess Plateau of China during the past four centuries. Sci Rep 7:7078
Tan LC, Cai YJ, Cheng H, Edwards RL, Shen CC, Gao Y, An ZS (2015) Climate significance of speleothem δ^{18}O from central China on decadal timescale. J Asian Earth Sci 106:150–155
Tan LC, Cai Y, An ZS, Cheng H, Shen CC, Gao YL, Edwards RL (2016) Decreasing monsoon precipitation in southwest China during the last 240 years associated with the warming of tropical ocean. Clim Dyn 48(5–6):1769–1778
Tao S, Chen L (1987) A review of recent research on the East Asian summer monsoon in China. In: Chang CP, Krisnamurti TN (eds) Monsoon meteorology. Oxford University Press, Oxford, pp 60–92
Tierney JE, Abram NJ, Anchukaitis KJ, Evans MN, Giry C, Kilbourne KH, Saenger CP, Wu HC, Zinke J (2015) Tropical sea surface temperatures for the past four centuries reconstructed from coral archives. Paleoceanography 30(3):226–252
Van LH, Meehl GS (2012) The Indian summer monsoon during peaks in the 11 year sunspot cycle. Geophys Res Lett 39(13):13701
Van LH, Meehl GA, Arblaster JM (2004) A decadal solar effect in the tropics in July–August. J Atmos Solar Terr Phys 66(18):1767–1778
Vecchi GA, Soden BJ, Wittenberg AT, Held IM, Leetmaa A, Harrison MJ (2006) Weakening of tropical Pacific atmospheric circulation due to anthropogenic forcing. Nature 441(7089):73–76
Wang B, Wu R, Fu X (2000) Pacific–East Asian teleconnection: how does ENSO affect East Asian climate? J Clim 13(9):1517–1536
Wang YJ, Cheng H, Edwards RL, An ZS, Wu JY, Shen CC, Dorale JA (2001) A high-resolution absolute-dated late Pleistocene monsoon record from Hulu Cave, China. Science 294:2345–2348
Wang YJ, Cheng H, Edwards RL, He Y, Kong XG, An ZS, Wu JY, Kelly M, Dykoski CA, Li XD (2005) The Holocene Asian monsoon: links to solar changes and North Atlantic climate. Science 308:854–857
Wang YJ, Cheng H, Edwards RL, Kong XG, Shao XH, Chen ST, Wu JY, Jiang XY, Wang XF, An ZS (2008) Millennial- and orbital-scale changes in the east asian monsoon over the past 224,000 years. Nature 451(7182):1090–1093
Wang B, Xiang B, Lee JY (2013) Subtropical high predictability establishes a promising way for monsoon and tropical storm predictions. Proc Natl Acad Sci 110(8):2718–2722
White WB, Liu Z (2008) Resonant excitation of the quasi-decadal oscillation by the 11-year signal in the sun's irradiance. J Geophys Res Oceans 113:C1
White WB, Lean J, Cayan DR, Dettinger MD (1997) Response of global upper ocean temperature to changing solar irradiance. J Geophys Res Oceans 102(C2):3255–3266
Wu GX, Liu YM (2003) Summer time quadruplet heating pattern in the subtropics and the associated atmospheric circulation. Geophy Res Lett 30:1201–1204
Wu GX, Liu YM, Ren RC, Liu P (2004) Relation between subtropical anticyclone and vertical motion in steady state. SCTS Met Sin 62(5):587–597 **(in Chinese with English abstract)**

Wu GX, Liu YM, Zhu X, Li W, Ren R, Duan S, Liang X (2009) Multi-scale forcing and the formation of subtropical desert and monsoon. Ann Geophys 27:3631–3644

Wu B, Li T, Zhou TJ (2010) Relative contributions of the Indian ocean and local SST anomalies to the maintenance of the western north Pacific anomalous anticyclone during the El Niño decaying summer. J Clim 23(11):2974–2986

Xie SP, Hafner J, Tokinaga H, Du Y, Huang G, Sampe T (2009) Indian ocean capacitor effect on Indo-Western Pacific climate during the summer following El Niño. J Clim 22(3):730–747

Yang JL, Liu QY, Xie SP, Liu ZY, Wu LX (2007) Impact of the Indian ocean SST basin mode on the Asian summer monsoon. Geophys Res Lett 34(2):155–164

Yang Y, Yuan D, Cheng H, Zhang ML, Qin JM, Lin YS, Zhu XY, Edwards RL (2010) Precise dating of abrupt shifts in the Asian Monsoon during the last deglaciation based on stalagmite data from Yamen Cave, Guizhou Province, China. Sci China Earth Sci 53(5):633–641

Yang R, Xie Z, Cao J (2017) A dynamic index for the westward ridge point variability of the western pacific subtropical high during summer. J Clim 30(9):3325–3341

Ye DZ, Gao YX (1979) Meteorology over Tibetan Plateau. Science Press, Beijing, p 278

Ye DZ, Wu GX (1998) The role of the heat source of the Tibetan Plateau in the general circulation. Meteorol Atmos Phys 67:181–198

Yuan DX, Cheng H, Edwards RL, Dykoski CA, Kelly MJ, Zhang ML, Qing JM, Lin YS, Wang YJ, Wu JY, Dorale JA, An ZS, Cai YJ (2004) Timing, duration, and transitions of the last interglacial Asian monsoon. Science 304:575–578

Zhang PZ, Cheng H, Edwards RL, Chen F, Wang Y, Yang XL, Liu J, Tan M, Wang XF, Liu JH, An CL, Dai ZB, Zhou J, Zhang DZ, Jia JH, Jin LY, Johnson KR (2008) A test of climate, sun, and culture relationships from an 1810-year Chinese cave record. Science 322:940–942

Zhang YH, Yang Y, Yang XL, Yin JJ, Huang F, Reng XF, Zhao JY, Liu X, Nie XD (2015) Early Holocene monsoon evolution of high-resolution stalagmite $\delta^{18}O$ records: in Henan Laomu Cave. Acta Sedimentol Sin 33(1):134–141 **(in Chinese with English abstract)**

Zhao ZG (1999) Summer drought and flood in China and the circulation over continent of Asia in summer (in Chinese). China Meteorological Press, Beijing, pp 45–46

Zhao K, Wang YJ, Edwards RL, Cheng H, Liu D (2010) High-resolution stalagmite $\delta^{18}O$ records of Asian monsoon changes in central and southern China spanning the MIS 3/2 transition. Earth Planet Sci Lett 298(1):191–198

Zhao JY, Yang Y, Peng T, Guo YW, Ren XF, Zhang YH, Nie XD, Liu X, Li JC, Ling XY, Zhang ZQ (2014) Variation of $\delta^{18}O$ values in the precipitation, cave drip water and modern calcite deposition in Jiguan Cave, Henan Province and its atmospheric circulation effect. Quat Sci 34:1106–1116 **(in Chinese with English abstract)**

Zhao K, Wang YJ, Edwards RL, Cheng H, Liu D, Kong X (2015) A high-resolved record of the Asian summer monsoon from Dongge Cave, China for the past 1200 years. Quat Sci Rev 122:250–257

Zhou TJ, Yu R, Zhang J, Drange H, Cassou C, Deser C, Hodson DLR, Sanchez-Gomez E, Li J, Keenlyside N, Xin XG, Okumura Y (2009) Why the Western Pacific subtropical high has extended westward since the late 1970s. J Clim 22(8):2199–2215